Chemical Science

ROYAL SOCIETY OF CHEMISTRY

EDGE ARTICLE

View Article Online
View Journal

Cite this: DOI: 10.1039/d6sc00358c

All publication charges for this article have been paid for by the Royal Society of Chemistry

Received 14th January 2026
Accepted 20th March 2026

DOI: 10.1039/d6sc00358c

rsc.li/chemical-science

Modular assembly of chiral biaryl phosphoramidite (BPA) libraries by nickel catalysis

Xi Zhang,† Jingyi Bai,† Yue Zhao, Minyan Wang and Zhuangzhi Shi *

Chiral phosphoramidites have emerged as pivotal ligands in asymmetric catalysis, yet their synthesis has long been constrained by traditional *de novo* approaches. Here, we present a highly significant late-stage functionalization strategy, which facilitates the modular assembly of biaryl phosphoramidite (BPA) libraries. Leveraging P(III)-directed C–H activation by nickel catalysis, we have developed a versatile platform for facile modification of the chiral pocket within these BPAs, enabling rapid structural optimization and exploration of diverse chemical architectures. These formed ligand libraries have demonstrated exceptional performance across a spectrum of asymmetric palladium-catalysed reactions, underscoring their broad applicability and potential. Through a synergistic combination of experimental investigations and computational analyses, we have elucidated the underlying reaction mechanism with remarkable clarity. This research not only furnishes advanced synthetic tools for the preparation of phosphoramidite libraries but also sets a new benchmark for the design and synthesis of novel ligands using state-of-the-art synthetic methodologies.

Introduction

Transition-metal-catalysed asymmetric catalysis has profoundly reshaped modern synthetic chemistry, offering unparalleled precision and diversity in stereoselective transformations. Central to this progress is the strategic design of privileged chiral ligands, which provide exceptional control over regio-, diastereo-, and enantioselectivity.[1] A pivotal milestone was achieved in 1994 with Feringa's development of MonoPhos, a groundbreaking chiral phosphoramidite ligand featuring a BINOL scaffold with a NMe_2 motif (Fig. 1a).[2] This ligand demonstrated unprecedented enantioselectivity in copper-catalysed conjugate additions of dialkyl zinc reagents to enones.[3] This impressive achievement inspired extensive research into chiral phosphoramidite derivatives based on the BINOL framework, setting a new benchmark in asymmetric catalysis.[4] However, the synthesis of phosphoramidites remains largely confined to traditional methods. These *de novo* approaches, which involve P–O or P–N bond formation through chlorophosphite synthesis, dichloroaminophosphine formation, or amine exchange, are often hindered by complex procedures, multi-step syntheses, and limited structural diversity.[5] These challenges underscore the urgent need for more efficient and versatile synthetic methods to expand the accessibility of chiral phosphoramidite libraries and facilitate precise ligand optimization for targeted catalytic applications.

Over the past decades, transition-metal-catalysed C–H activation has emerged as a transformative strategy in organic synthesis, offering unparalleled efficiency and selectivity in modifying carbon centers.[6] Since the early 2000s, serendipitous discoveries have highlighted the potential of phosphoramidite ligands in this context (Fig. 1b). In 2003, Hartwig *et al.* reported a significant result where a metallacyclic iridium-phosphoramidite, formed *via* aliphatic C–H activation *in situ*, served as the active supporting ligand in iridium-catalysed kinetic asymmetric substitution of racemic allylic electrophiles.[7] This discovery was further advanced by You and co-workers, who identified that the iridicycle is generated through aromatic C–H activation of the *N*-aryl group within the ligand, a key active species in many iridium-catalysed asymmetric allylic alkylation reactions.[8] These findings were initially limited to stoichiometric transformations, where the metal and ligand are used in equimolar amounts. However, developing a catalytic process using small amounts of transition metals with stoichiometric phosphoramidites remains challenging due to the highly electron-rich and strongly coordinating nature of the P(III) center in these compounds.

Recent advancements have underscored the transformative potential of P(III)-directed C–H activation in catalytic processes.[9] A pivotal development in this field has been the strategic incorporation of $N–PR_2$ groups, which has demonstrated remarkable efficacy in enhancing regioselectivity and functional group tolerance (Fig. 1c). The attachment of the P^tBu_2 moiety to the nitrogen atom of indole facilitates C–H arylation at the C7 position with aryl bromides or carboxylic acid anhydrides, a regioselectivity that is often elusive with conventional

State Key Laboratory of Coordination Chemistry, Chemistry and Biomedicine Innovation Center (ChemBIC), School of Chemistry and Chemical Engineering, Nanjing University, Nanjing 210093, China. E-mail: shiz@nju.edu.cn

† These authors contributed equally to this work.

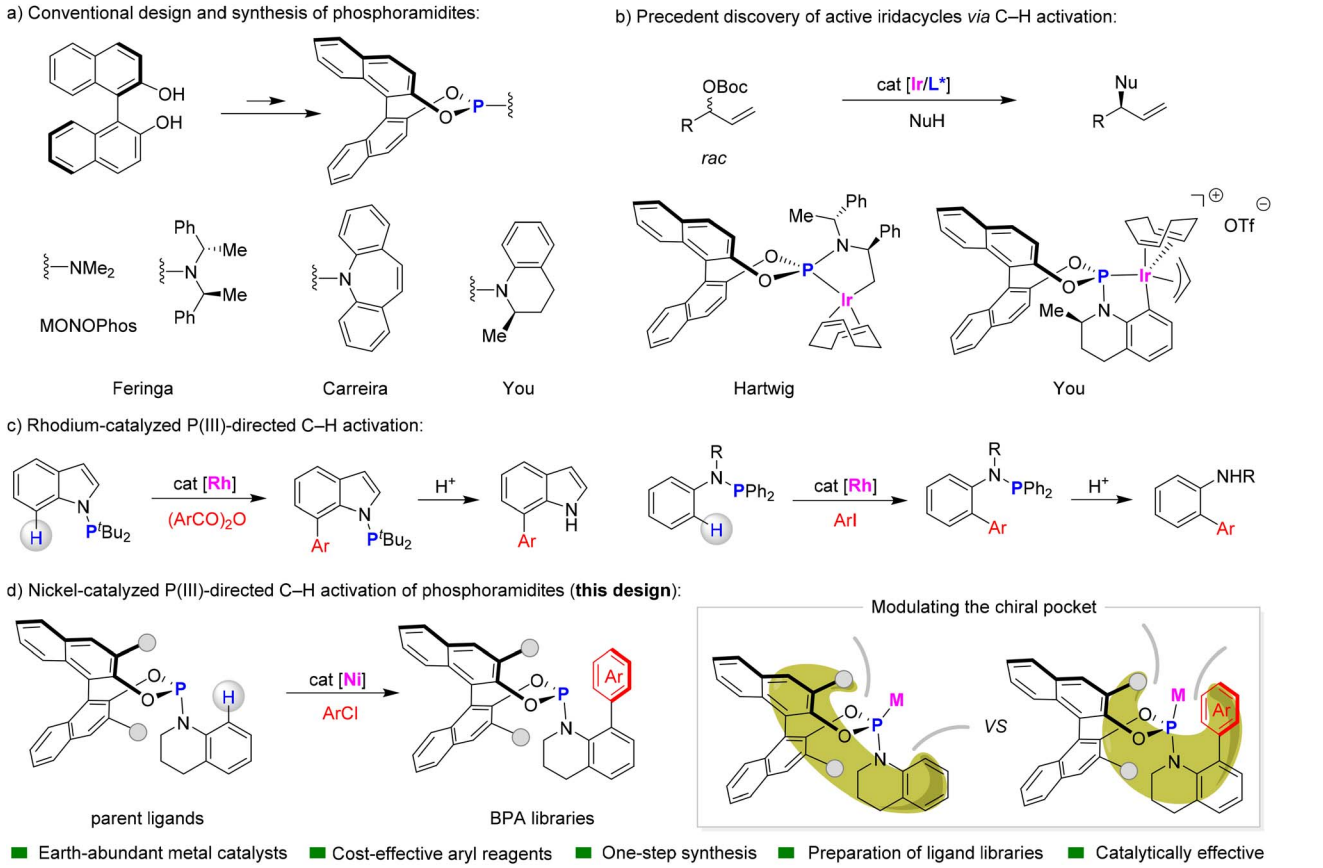

Fig. 1 Background and this discovery.

directing groups.[10] Moreover, the recent work by Evano and Lan has introduced a protocol for P(III)-directed *ortho*-selective C–H arylation of amino-phosphines using aryl iodides under rhodium catalysis.[11] This method offers significant practical advantages, as the N-PR_2 group can be readily removed under mild acidic conditions to yield NH-free products. Despite these advancements, current methodologies are predominantly constrained by their reliance on precious metal catalysts, and the removal of directing groups from the nitrogen atom does not fully leverage the inherent P(III) functionality.

Here, we present a highly efficient catalytic system for P(III)-directed C–H activation of phosphoramidites, which enables the modular assembly of chiral ligand libraries (Fig. 1d). This innovative approach utilizes a nickel catalyst to facilitate the efficient coupling of diverse aryl chlorides, constructing biaryl phosphoramidite (BPA) libraries with exceptional efficiency. The choice of nickel, a more abundant and cost-effective metal compared to iridium, significantly enhances the scalability and industrial applicability of this methodology.[12] Additionally, the use of aryl chlorides, which are more economical and readily available than their bromo and iodo counterparts, highlights the practical and economic advantages of this approach. Notably, when Pd catalysis is employed with aryl iodides, a C–P coupling reaction of phosphoramidites occurs instead of C–H activation, resulting in the formation of P-chirogenic compounds.[13] Through the implementation of late-stage functionalization strategies, we can modulate the chiral pocket of the formed BPA libraries, enabling rapid reaction optimization and the exploration of diverse chemical space.

Results and discussion

Reaction design

To optimize the reaction conditions, we initiated our study using enantiomerically enriched phosphoramidite **1a** with 99% ee (enantiomeric excess) and aryl chloride **2a** as model substrates, both of which are commercially available (Table 1). The reaction was first performed in the presence of $[Ir(cod)Cl]_2$ (5.0 mol%) and LiO^tBu (2.0 equivalents) in toluene at 110 °C for 48 hours in a N_2 atmosphere. However, no desired product was observed, highlighting the significant difference between stoichiometric and catalytic processes (entry 1). Switching to $[Rh(cod)Cl]_2$ instead of $[Ir(cod)Cl]_2$ yielded a small amount of the desired product **BPA1** (entry 2). Further screening of metal catalysts revealed that $Ni(cod)_2$ significantly enhanced the reaction, increasing the yield of **BPA1** to 42% (entry 3). Next, we explored the influence of ligands on the reaction. Using PPh_3 as a ligand slightly improved the yield to 46% (entry 4). However, the electron-rich ligand P(2-OMe-Ph)$_3$ was detrimental to the reaction (entry 5). In contrast, electron-deficient phosphine ligands such as P(2-F-Ph)$_3$ favored product formation (entry 6). Further investigation showed that P(3-F-Ph)$_3$ boosted the yield

Table 1 Reaction discovery and optimization[a]

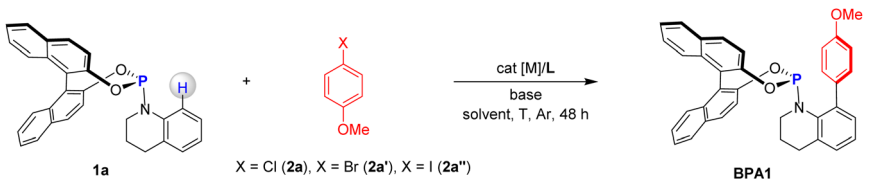

Entry	X	cat [M] (mol%)	L (mol%)	Base (equiv.)	Solvent	T (°C)	Yield of BPA1[b] (%)
1	Cl (**2a**)	$[Ir(cod)Cl]_2$ (5)	—	LiO^tBu (3.0)	Toluene	110	0
2	Cl (**2a**)	$[Rh(cod)Cl]_2$ (5)	—	LiO^tBu (3.0)	Toluene	110	<5
3	Cl (**2a**)	$Ni(cod)_2$ (10)	—	LiO^tBu (3.0)	Toluene	110	42
4	Cl (**2a**)	$Ni(cod)_2$ (10)	PPh_3 (20)	LiO^tBu (3.0)	Toluene	110	46
5	Cl (**2a**)	$Ni(cod)_2$ (10)	P(2-OMe-Ph)$_3$ (20)	LiO^tBu (3.0)	Toluene	110	38
6	Cl (**2a**)	$Ni(cod)_2$ (10)	P(2-F-Ph)$_3$ (20)	LiO^tBu (3.0)	Toluene	110	45
7	Cl (**2a**)	$Ni(cod)_2$ (10)	P(3-F-Ph)$_3$ (20)	LiO^tBu (3.0)	Toluene	110	55
8	Cl (**2a**)	$Ni(cod)_2$ (10)	P(4-F-Ph)$_3$ (20)	LiO^tBu (3.0)	Toluene	110	37
9	Cl (**2a**)	$Ni(cod)_2$ (10)	P(4-CF_3-Ph)$_3$ (20)	LiO^tBu (3.0)	Toluene	110	52
10	Cl (**2a**)	$Ni(cod)_2$ (10)	P(3,5-CF_3-Ph)$_3$ (20)	LiO^tBu (3.0)	Toluene	110	64
11	Cl (**2a**)	$Ni(cod)_2$ (10)	P(3,5-CF_3-Ph)$_3$ (20)	KO^tBu (3.0)	Toluene	110	<5
12	Cl (**2a**)	$Ni(cod)_2$ (10)	P(3,5-CF_3-Ph)$_3$ (20)	NaO^tBu (3.0)	Toluene	110	<10
13	Cl (**2a**)	$Ni(cod)_2$ (10)	P(3,5-CF_3-Ph)$_3$ (20)	Li_2CO_3 (3.0)	Toluene	110	0
14	Cl (**2a**)	$Ni(cod)_2$ (10)	P(3,5-CF_3-Ph)$_3$ (20)	LiO^tBu (3.0)	1,4-Dioxane	110	<5
15	Cl (**2a**)	$Ni(cod)_2$ (10)	P(3,5-CF_3-Ph)$_3$ (20)	LiO^tBu (3.0)	Toluene	130	55
16	Cl (**2a**)	$Ni(cod)_2$ (10)	P(3,5-CF_3-Ph)$_3$ (20)	LiO^tBu (3.0)	Toluene	90	51
17	Cl (**2a**)	$NiBr_2$ (10)	P(3,5-CF_3-Ph)$_3$ (20)	LiO^tBu (3.0)	Toluene	110	<10
18	Cl (**2a**)		P(3,5-CF_3-Ph)$_3$ (20)	LiO^tBu (3.0)	Toluene	110	0
19	Br (**2a′**)	$Ni(cod)_2$ (10)	P(3,5-CF_3-Ph)$_3$ (20)	LiO^tBu (3.0)	Toluene	110	40
20	I (**2a″**)	$Ni(cod)_2$ (10)	P(3,5-CF_3-Ph)$_3$ (20)	LiO^tBu (3.0)	Toluene	110	18

[a] Reaction conditions: cat [M] (5.0–10.0 mol%), L (20.0 mol%), **1a** (0.10 mmol), **2a** (0.30 mmol), and base (0.30 mmol) in 1.0 mL of toluene, at 110 °C for 48 hours under nitrogen. [b] Isolated yield.

to 55% (entry 7), while P(4-F-Ph)$_3$ reduced reactivity (entry 8). Interestingly, P(4-CF_3-Ph)$_3$ provided a higher yield of 52% (entry 9), and P(3,5-CF_3-Ph)$_3$ gave the best result, achieving a 64% yield of **BPA1** (entry 10). We then examined the role of different bases. Replacing LiO^tBu with KO^tBu or NaO^tBu drastically reduced the yield of **BPA1**, and Li_2CO_3 completely inhibited the reaction (entries 11–13). These results underscore the critical roles of both Li^+ and O^tBu^- ions in the efficient conversion of the substrates. Solvent optimization studies demonstrated that replacing toluene with 1,4-dioxane led to a sharp decrease in reactivity (entry 14). We also screened reaction temperatures. Both increasing (130 °C) and decreasing (90 °C) the temperature resulted in reduced reactivity (entries 15–16). To further explore the impact of the catalyst, we tested other nickel catalysts, such as $NiBr_2$, which exhibited much lower activity compared to $Ni(cod)_2$ (entry 17). A control experiment confirmed that the reaction did not proceed in the absence of the catalyst, emphasizing its essential role (entry 18). Additionally, replacing aryl chloride **2a** with aryl bromide **2a′** and iodide **2a″** resulted in significantly lower yields (entries 19–20), highlighting the unique reactivity of the C–Cl bond in this transformation. Notably, all the above reactions proceeded with excellent retention of chirality, affording the product **BPA1** with 99% es.

Reaction scope

To comprehensively assess the versatility of the reaction, we initiated our investigation by examining the scope of aryl chlorides with phosphoramidite **1a** (Table 2). The reaction involving chlorobenzene (**2b**) yielded **BPA2** with a 68% yield and an es exceeding 99%. Aryl chlorides featuring alkyl substituents, including methyl (**2c**, **2d**), ethyl (**2e**), *n*-butyl (**2f**), and *tert*-butyl (**2g**), proved to be compatible with the transformation, producing the desired products **BPA2** to **BPA7** in moderate yields while maintaining high enantioselectivities. Substrates with electron-donating groups, such as methoxy (**2h**), dioxole (**2i**), and methylthio (**2j**), underwent smooth reactions, yielding **BPA8** to **BPA10**. The structure of product **BPA8** was unequivocally confirmed through X-ray crystallographic analysis. Aryl chlorides bearing electron-withdrawing substituents, such as fluorine (**2k**, **2l**) and trifluoromethyl (**2m**, **2n**), also exhibited favorable outcomes, efficiently yielding **BPA11** to **BPA14**. The reaction with aryl chloride **2o**, which contains a sensitive olefinic group, was compatible, affording the corresponding product **BPA15** in 53% yield with an es value surpassing 99%. Given the capability to rapidly modulate the steric and electronic properties of the ligand by incorporating diverse aryl motifs, substrates with biphenyl (**2p**) and naphthalen-2-yl (**2q**) reacted efficiently, yielding **BPA16** and **BPA17** with consistent

Table 2 Scope of the BPA libraries[a]

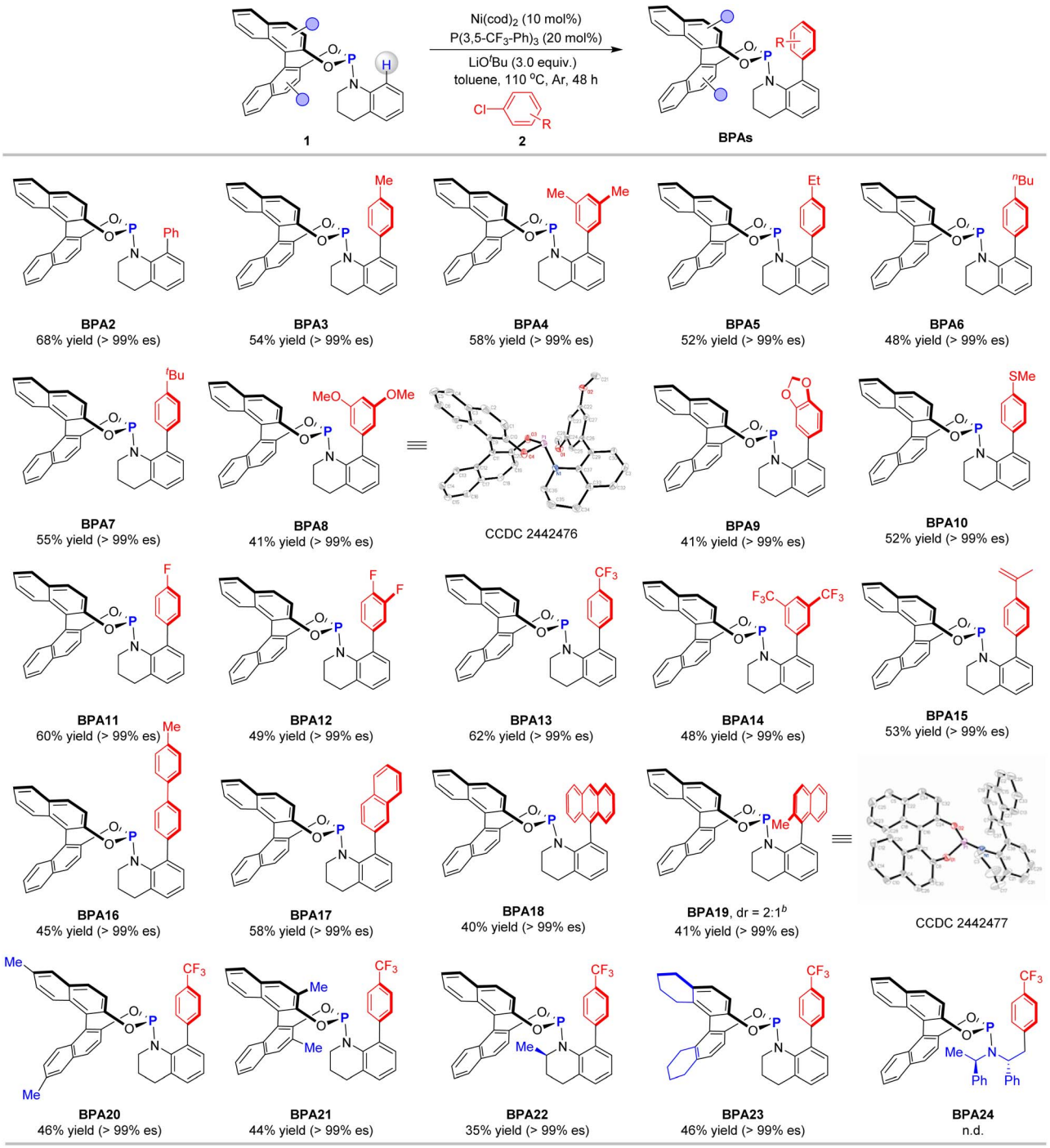

[a] Reaction conditions: $Ni(cod)_2$ (10.0 mol%), $P(3,5\text{-}CF_3\text{-}Ph)_3$ (20.0 mol%), **1** (0.10 mmol), **2** (0.30 mmol), and LiO^tBu (0.3 mmol) in 1.0 mL of toluene, at 110 °C for 48 hours under nitrogen. [b] The value of dr was determined by isolated yield.

enantiospecificity. The reaction involving the sterically hindered substrate 9-chloroanthracene (**2r**) with **1a** afforded **BPA18** in modest yield with excellent enantiospecificity. When 1-chloro-2-methylnaphthalene was employed as the substrate, the reaction yielded only 30% of the product. However, using the corresponding bromide **2s** resulted in a 41% yield of **BPA19**, which comprised a pair of diastereomers in a 2 : 1 ratio. One of these diastereomers was successfully isolated, and its absolute configuration was unequivocally determined through X-ray crystallographic analysis. Using 1-chloro-4-(trifluoromethyl) benzene (**2m**) as the substrate, we further investigated the influence of substituents on the Binol moiety. When

phosphoramidites **1b** and **1c**, bearing methyl groups at the 6, 6′ and 3, 3′ positions, respectively, were employed, the desired products **BPA20** and **BPA21** were successfully obtained. Additionally, phosphoramidite **1d**, featuring a 2-methyl-1,2,3,4-tetrahydroquinoline motif, was compatible with the reaction, only yielding the aromatic C–H arylation product **BPA22**. Beyond the binol motif, the use of 8H-binol-derived phosphoramidite **1e** in the reaction also resulted in the formation of **BPA23** in 46% yield, with retained enantiospecificity. In contrast, ligands bearing amine-derived motifs—such as Feringa's ligand containing the bis(1-phenylethyl)amine moiety (**BPA24**)[14] and Carreira's ligand—proved entirely ineffective under the current conditions. It is worth noting that only moderate yields were obtained for several of these products, primarily due to the susceptibility of the phosphoramidite ligands to oxidation, necessitating rapid chromatographic purification. In addition, the presence of trace water in the reaction system could lead to product hydrolysis, further impacting the yields.

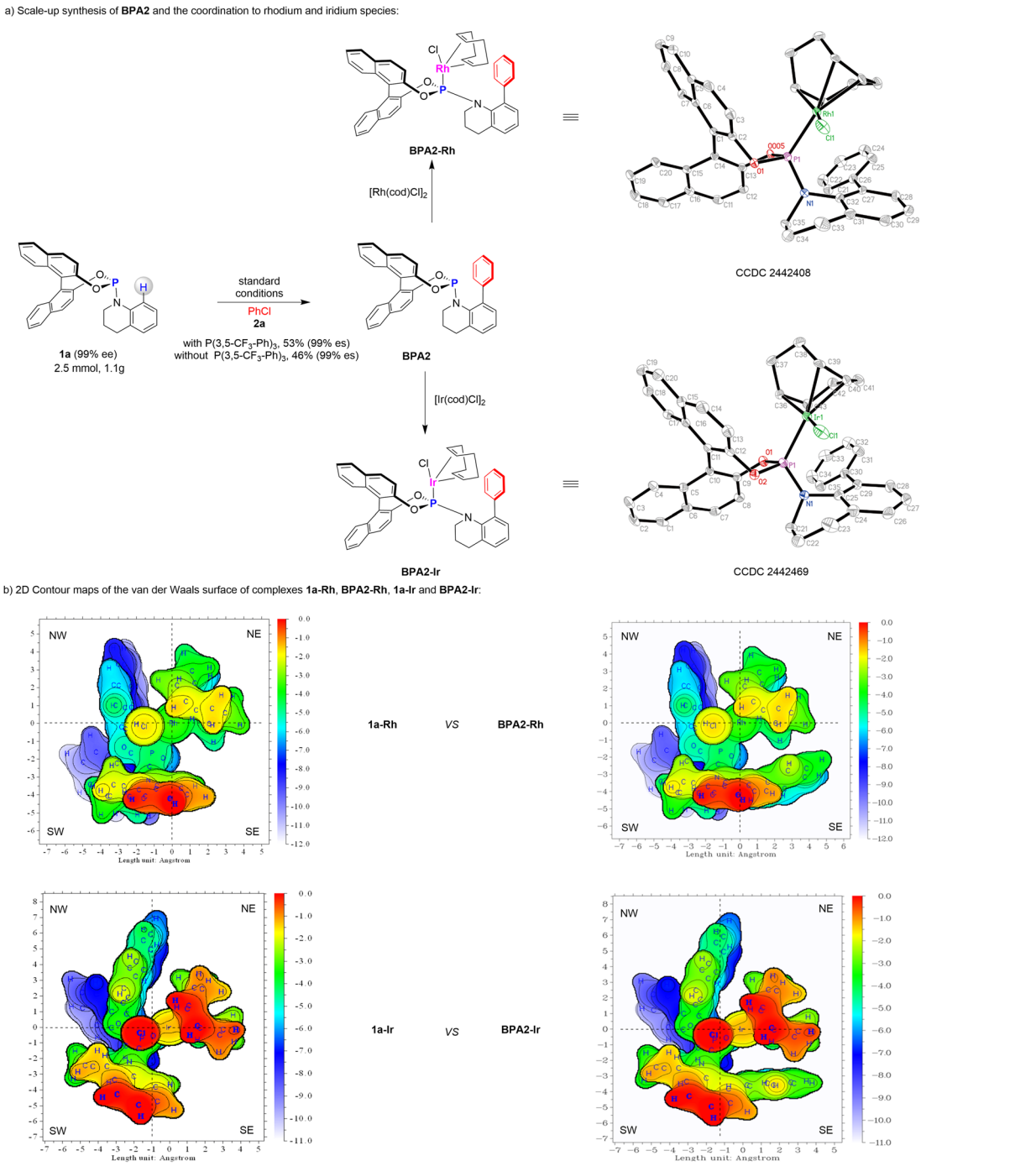

Fig. 2 Further investigations of the crystal model.

Synthetic applications

The developed strategy has demonstrated remarkable efficiency in the synthesis of BPA libraries, representing a novel approach in the development of efficient chiral phosphoramidite ligands for catalysis and organometallic reactivity (Fig. 2). When the reaction of phosphoramidite **1a** was scaled up to 2.5 mmol with PhCl (**2b**), the desired product **BPA2** was obtained in 53% yield without significant loss in efficiency under standard conditions (Fig. 2a). Further investigations revealed that, even in the absence of the ligand, the corresponding product could still be obtained in 46% yield. This finding underscores that the primary role of the ligand is to enhance reaction efficiency rather than being a critical factor for the transformation itself. When 1.0 equivalent of **BPA2** was allowed to react with a stoichiometric amount of $[Rh(cod)Cl]_2$ or $[Ir(cod)Cl]_2$, complexes **BPA2-Rh** and **BPA2-Ir** were obtained, respectively. X-ray crystallographic analysis revealed that the metal centers in both complexes are chelated solely by the phosphorus atom. For **BPA2-Rh**, the bond lengths and angles surrounding the Rh atom range from 2.118(4) to 2.3597(11) Å and 35.16(15) to 120.06(13)°, respectively. Similarly, the reaction with $[Ir(cod)Cl]_2$ yielded a monometallic complex, **BPA2-Ir**, where the iridium center is chelated by P, C, and Cl atoms. The Ir-centered bond lengths and angles in **BPA2-Ir** range from 2.113(8) to 2.356(2) Å and 36.0(3) to 120.0(3)°, respectively. To better illustrate the steric repulsions at different regions of the formed ligands, the structural and spatial characteristics of the phosphoramidite complexes were systematically investigated using Multiwfn[15] to generate detailed two-dimensional (2D) contour maps (Fig. 2b).[16] The analysis revealed distinct differences in the spatial arrangements between the Rh and Ir complexes of **1a** and their phenyl-substituted counterparts (**BPA2-Rh** and **BPA2-Ir**). The complexes **1a-Rh** and **1a-Ir** were found to create a relatively open and accessible environment for substrate binding. However, a significant structural modification was observed upon the introduction of a phenyl group into the ligand framework. The phenyl group in **BPA2-Rh** and **BPA2-Ir** was found to project into the southeast (SE) quadrant of the spatial environment, creating a pronounced steric effect around the metal center. As a direct consequence, the cavity around the metal that can accommodate the substrate becomes notably smaller. This reduction in the cavity size likely facilitates more pronounced ligand–substrate interactions, leading to the emergence of unique selectivity in the reaction system.

Based on the above results, we then evaluated their potential in asymmetric catalysis (Fig. 3). We chose parent ligand **1a**, with the representative products **BPA1**, **BPA2**, **BPA13**, **BPA18**, **BPA21** and **BPA23**—each distinguished by unique steric and electronic properties, to generate a small ligand library and tested them

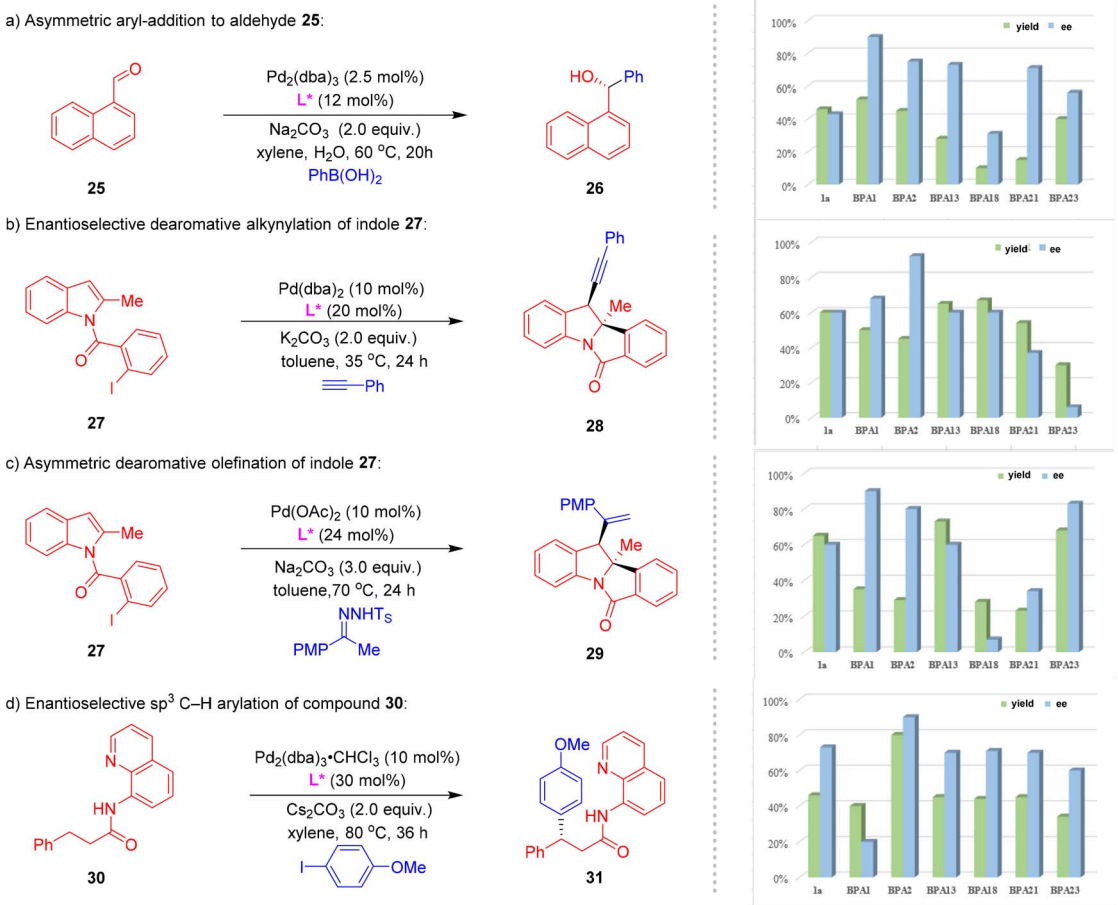

Fig. 3 Investigating some BPAs in asymmetric catalysis.

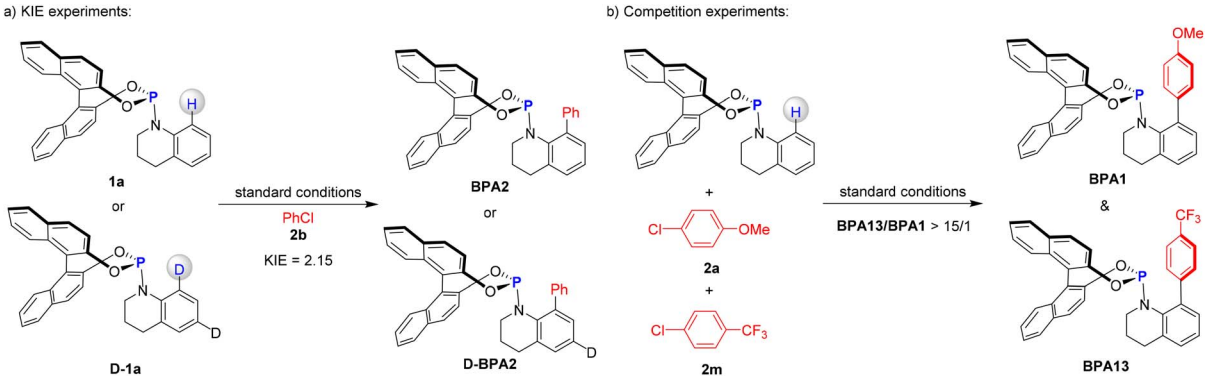

Fig. 4 Mechanistic experiments.

for asymmetric catalysis. In our experimental investigation, we first evaluated the performance of our ligands in the asymmetric addition of phenylboric acid to aldehyde **25** (Fig. 3a).[17] Initially, using the parent ligand **1a**, the reaction yielded product **26** with a modest 46% yield and 43% ee. Subsequent screening of the developed ligands revealed that **BPA1** emerged as the optimal ligand, significantly enhancing the reaction outcome to 52% yield and 90% ee. Building on these promising results, we extended our study to the enantioselective dearomative difunctionalization of indoles—a highly valuable strategy for constructing complex chiral *N*-heterocycles (Fig. 3b).[18] The catalytic performance of these ligands was assessed in the palladium-catalysed enantioselective cycloaddition of indole **27** with phenylacetylene. Remarkably, ligand **BPA2** demonstrated exceptional efficacy, delivering product **28** in 45% yield and 91% ee, thereby significantly outperforming the parent ligand **1a**. Moreover, **BPA13** exhibited a higher reactivity but low enantioselectivity, resulting in product **29** in 73% yield and 60% ee. To further explore the potential applications of BPAs, we investigated a Pd-catalysed dearomative arylvinylation of indoles **27**, utilizing *N*-arylsulfonyl hydrazones as versatile coupling partners to access 3-vinylindolines derivative **29** (Fig. 3c).[19] In contrast to the moderate enantioselectivity displayed by **1a**, **BPA1** proved to be highly effective, achieving an ee value of 90%. Furthermore, **BPA23** also yielded a relatively good result, although it was not the optimal ligand. Finally, we applied the ligand library to a Pd-catalysed asymmetric sp^3 C–H activation of compound **30** with4-OMe-iodobenzene to afford product **31** (Fig. 3d).[20] Remarkably, ligand **BPA2** significantly increased the enantioselectivity to 90% ee, representing a substantial improvement over the parent ligand **1a**. These results unequivocally demonstrate the versatility and efficacy of the newly developed BPA libraries, as evidenced by their broad applicability and enhanced performance across a variety of challenging asymmetric transformations.

Mechanistic studies

Subsequent mechanistic studies provided critical insights into the pathway of the Ni-catalysed C–H arylation (Fig. 4). Initial experiments employing phosphine **1a** in conjunction with isotopically labeled substrate **D-1a** and PhCl (**2b**) revealed a significant primary kinetic isotope effect (KIE) of $k_H/k_D = 2.15$. This pronounced KIE value strongly implicates C–H bond cleavage as the rate-determining step in the catalytic cycle (Fig. 4a).[21] Further mechanistic elucidation was achieved through a parallel competition experiment between aryl chloride **1b** and **13b** (5.0 equiv. each) in the presence of phosphoramidite **1a** (1.0 equiv). The reaction yielded a mixture of **BPA13** and **BPA1** with more than 15/1 ratio (Fig. 4b). The pronounced selectivity toward the electron-deficient substrate **13b** highlights the significantly accelerated reaction rates with electrophiles bearing electron-withdrawing groups, consistent with a mechanism driven by nucleophilic aromatic substitution.[22] These experimental findings support the proposed mechanism, wherein oxidative addition of the aryl chloride to the Ni(0) complex is not the rate-determining step within the catalytic cycle.

To elucidate the reaction mechanism in greater detail, we conducted comprehensive density functional theory (DFT) calculations using phosphoramidite **1a** and aryl chloride **2a** as model substrates (Fig. 5).[23] The catalytic cycle initiates with a crucial step where the cod ligands of the $Ni(cod)_2$ precatalyst are displaced by substrate **1a** and the ligand, resulting in the formation of the highly reactive Ni(0) species **INT1A**. This species acts as the active catalyst in the subsequent transformations. Following this, **INT1A** coordinates with compound **2a**, leading to the exothermic formation of complex **INT2A**, with an exothermic energy of 14.4 kcal mol^{-1}. The oxidative addition of the C–Cl bond to the nickel center of **INT2A** proceeds through the transition state **TS1A**, which has an activation free energy of 13.8 kcal mol^{-1} (Fig. 5a). The base LiO^tBu can potentially initiate two competing pathways for C–H metalation.[24] Notably, the base-assisted outer-sphere concerted metalation-deprotonation pathway is energetically more favorable than the inner-sphere mechanism (14.6 kcal mol^{-1} for **TS2A** *vs.* 34.9 kcal mol^{-1} for **TS2B**, Fig. 5b). This significant energy difference strongly indicates that the base-assisted outer-sphere concerted metalation-deprotonation pathway is the predominant mechanism in this reaction. For the key transition state **TS2A**, the lengths of the C–Ni bond and the O–H bond, which are on the verge of formation, are measured to be 2.10 Å and 1.51 Å, respectively. Meanwhile, the length of the C–H bond about to be cleaved is determined to be 1.21 Å. The cleavage of the C–H bond represents the rate-determining step, which aligns with the experimentally observed kinetic isotope effect. The resulting

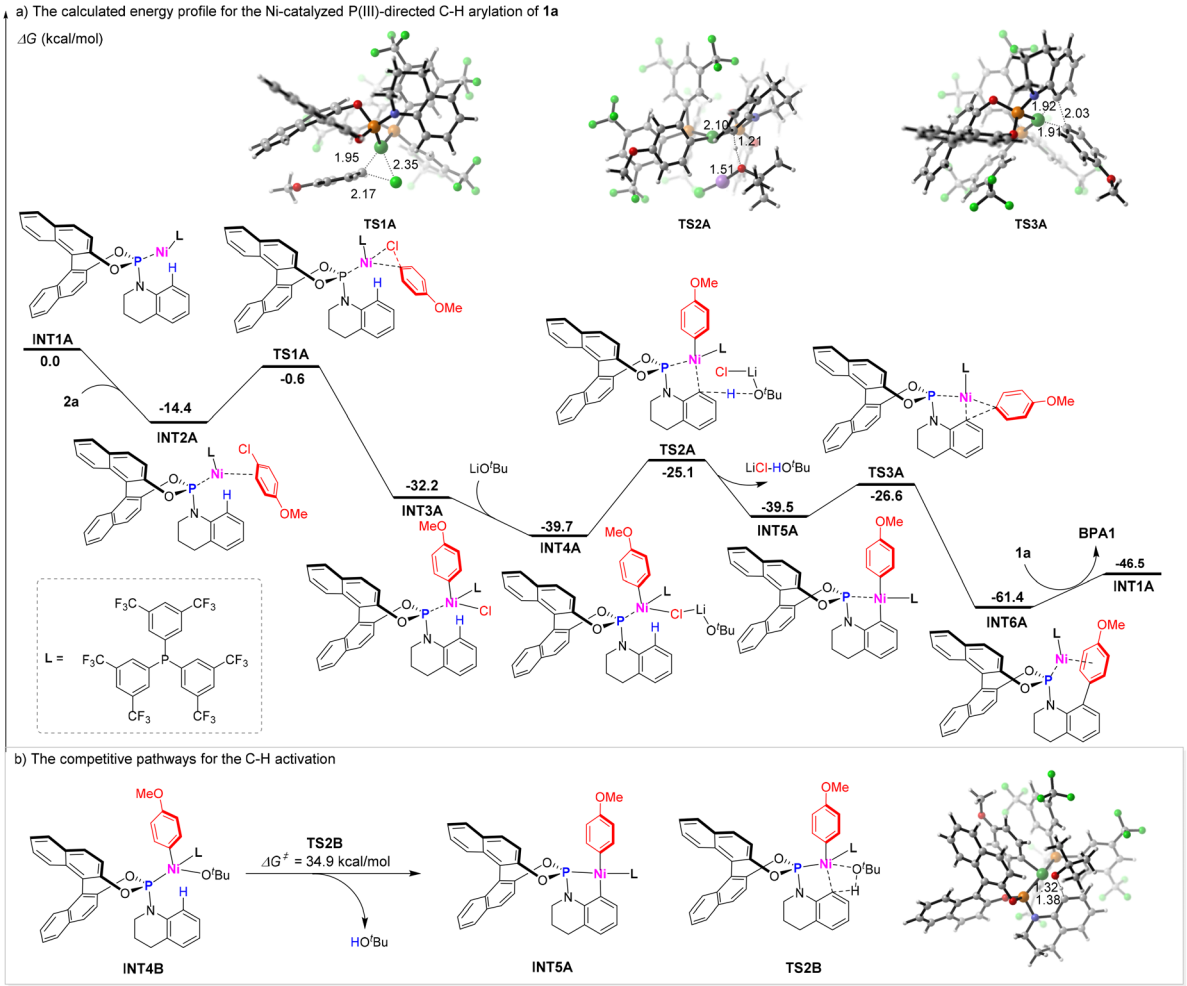

Fig. 5 Calculated energy profiles for the nickel-catalyzed P(III)-directed C–H arylation. All calculations were performed at the M06-D3/6-311+G(d,p)-SDD/SMD(toluene)//B3LYP-D3BJ/6-31G(d)-SDD level of theory using the Gaussian 09 software package.

nickelacycle intermediate **INT5A** undergoes reductive elimination *via* transition state **TS3A**, with a calculated barrier of 12.9 kcal mol^{-1}, leading to the formation of intermediate **INT6A**. Finally, ligand exchange occurs, a process that efficiently regenerates the active Ni(0) species **INT1A** and simultaneously releases the desired product **BPA1**, thereby completing the catalytic cycle.

Conclusions

In summary, we developed a modular late-stage functionalization strategy for synthesizing BPA libraries, enabling efficient structural diversification of chiral phosphoramidite ligands. Leveraging nickel-catalysed P(III)-directed C–H activation, we achieved rapid optimization of the chiral pocket, resulting in ligand libraries with exceptional performance in palladium-catalysed asymmetric reactions. Combined experimental and computational insights clarified the reaction mechanisms, providing a foundation for future ligand design. This approach sets a new standard for ligand synthesis and opens avenues for developing next-generation chiral catalysts. Future work could expand this strategy to other ligand systems, explore new catalytic applications, and integrate computational tools for accelerated discovery.

Author contributions

X. Z. performed the experiments, conducted the mechanistic studies, and analyzed the data. J. B. & M. W. performed the DFT calculations. Y. Z performed the crystallographic studies. Z. S. designed the study and wrote the manuscript.

Conflicts of interest

There are no conflicts to declare.

Data availability

CCDC 2442475 (**BPA8**), 2442477 (**BPA19**), 2442408 (**BPA2-Rh**), and 2442469 (**BPA2-Ir**) contain the supplementary crystallographic data for this paper.[25a–d]

The data supporting this article have been included as part of the supplementary information (SI). Supplementary information: experimental procedures, characterizations, and

analytical data of new compounds, and spectra of NMR and HPLC for new compounds (PDF). See DOI: https://doi.org/10.1039/d6sc00358c.

Acknowledgements

We would like to acknowledge financial support from the National Key R&D Program of China (2022YFA1503200), the National Natural Science Foundation of China (92361201, 22025104 and 22171134), the Natural Science Foundation of Jiangsu Province (BK20240059, BK20220033), and the Fundamental Research Funds for the Central Universities (020514380352).

Notes and references

1 (*a*) Q.-L. Zhou, *Privileged Chiral Ligands and Catalysts*, Wiley-VCH, Weinheim, 2011; (*b*) T. Imamoto, *Chem. Rev.*, 2024, **124**, 8657–8739; (*c*) W. Fu and W. Tang, *ACS Catal.*, 2016, **6**, 4814–4858; (*d*) T. P. Yoon and E. N. Jacobsen, *Science*, 2003, **299**, 1691–1693.

2 R. Hulst, N. K. de Vries and B. L. Feringa, *Tetrahedron: Asymmetry*, 1994, **5**, 699–708.

3 (*a*) B. L. Feringa, M. Pineschi, L. A. Arnold, R. Imbos and A. H. M. de Vries, *Angew. Chem., Int. Ed.*, 1996, **35**, 2374–2376; (*b*) B. L. Feringa, M. Pineschi, L. A. Arnold, R. Imbos and A. H. M. de Vries, *Angew. Chem., Int. Ed.*, 1997, **36**, 2620–2623.

4 (*a*) B. L. Feringa, *Acc. Chem. Res.*, 2000, **33**, 346–353; (*b*) A. J. Minnaard, B. L. Feringa, L. Lefort and J. G. de Vries, *Acc. Chem. Res.*, 2007, **40**, 1267–1277; (*c*) J. F. Hartwig and L. M. Stanley, *Acc. Chem. Res.*, 2010, **43**, 1461–1475; (*d*) C.-X. Zhuo, C. Zheng and S.-L. You, *Acc. Chem. Res.*, 2014, **47**, 2558–2573; (*e*) S. L. Rössler, D. A. Petrone and E. M. Carreira, *Acc. Chem. Res.*, 2019, **52**, 2657–2672; (*f*) B. M. Trost and G. Mata, *Acc. Chem. Res.*, 2020, **53**, 1293–1305.

5 J. F. Teichert and B. L. Feringa, *Angew. Chem., Int. Ed.*, 2010, **49**, 2486–2528.

6 (*a*) R. Giri, B.-F. Shi, K. M. Engle, N. Maugel and J.-Q. Yu, *Chem. Soc. Rev.*, 2009, **38**, 3242–3272; (*b*) C. G. Newton, S.-G. Wang, C. C. Oliveira and N. Cramer, *Chem. Rev.*, 2017, **117**, 8908–8976; (*c*) C. Sambiagio, D. Schönbauer, R. Blieck, T. Dao-Huy, G. Pototschnig, P. Schaaf, T. Wiesinger, M. F. Zia, J. Wencel-Delord, T. Besset, B. U. W. Maes and M. Schnürch, *Chem. Soc. Rev.*, 2018, **47**, 6603–6743; (*d*) Ł. Woźniak, J.-F. Tan, Q.-H. Nguyen, A. M. d. Vigné, V. Smal, Y.-X. Cao and N. Cramer, *Chem. Rev.*, 2020, **120**, 10516–10543; (*e*) B. Liu, A. M. Romine, C. Z. Rubel, K. M. Engle and B.-F. Shi, *Chem. Rev.*, 2021, **121**, 14957–15074; (*f*) C.-X. Liu, W.-W. Zhang, S.-Y. Yin, Q. Gu and S.-L. You, *J. Am. Chem. Soc.*, 2021, **143**, 14025–14040; (*g*) Q. Zhang, L.-S. Wu and B.-F. Shi, *Chem*, 2022, **8**, 384–413.

7 (*a*) C. A. Kiener, C. Shu, C. Incarvito and J. F. Hartwig, *J. Am. Chem. Soc.*, 2003, **125**, 14272–14273; (*b*) C. Shu, A. Leitner and J. F. Hartwig, *Angew. Chem., Int. Ed.*, 2004, **43**, 4797–4800; (*c*) T. Graening and J. F. Hartwig, *J. Am. Chem. Soc.*, 2005, **127**, 17192–17193; (*d*) D. J. Weix and J. F. Hartwig, *J. Am. Chem. Soc.*, 2007, **129**, 7720–7721; (*e*) H. Qin, J. T. Lowe and J. S. Panek, *J. Am. Chem. Soc.*, 2007, **129**, 38–39; (*f*) S. T. Madrahimov, D. Markovic and J. F. Hartwig, *J. Am. Chem. Soc.*, 2009, **131**, 7228–7229; (*g*) S. T. Madrahimov and J. F. Hartwig, *J. Am. Chem. Soc.*, 2012, **134**, 8136–8147; (*h*) T. W. Butcher, J. L. Yang, W. M. Amberg, N. B. Watkins, N. D. Wilkinson and J. F. Hartwig, *Nature*, 2020, **583**, 548–553.

8 (*a*) W.-B. Liu, C. Zheng, C.-X. Zhuo, L.-X. Dai and S.-L. You, *J. Am. Chem. Soc.*, 2012, **134**, 4812–4821; (*b*) X. Zhang, W. Liu, Q. Cheng and S.-L. You, *Organometallics*, 2016, **35**, 2467–2472; (*c*) S. Rieckhoff, J. Meisner, J. Kästner, W. Frey and R. Peters, *Angew. Chem., Int. Ed.*, 2018, **57**, 1404–1408; (*d*) L. S. Hutchings-Goetz, C. Yang, J. W. B. Fyfe and T. N. Snaddon, *Angew. Chem., Int. Ed.*, 2020, **59**, 17556–17564.

9 (*a*) Z. Zhang, P. H. Dixneuf and J.-F. Soulé, *Chem. Commun.*, 2018, **54**, 7265–7280; (*b*) J. Zhang, L. Yao, J.-Y. Su, Y.-Z. Liu, Q. Wang and W. P. Deng, *Green Synth. Catal.*, 2023, **4**, 206–225; (*c*) Z. Li and Z. Shi, *Acc. Chem. Res.*, 2024, **57**, 1057–1072.

10 X. Qiu, P. Wang, D. Wang, M. Wang, Y. Yuan and Z. Shi, *Angew. Chem., Int. Ed.*, 2019, **58**, 1504–1508.

11 C. Jacob, J. Annibaletto, J. Peng, R. Bai, B. U. W. Maes, Y. Lan and G. Evano, *Angew. Chem., Int. Ed.*, 2024, **63**, e202403553.

12 S. Z. Tasker, E. A. Standley and T. F. Jamison, *Nature*, 2014, **509**, 299–309.

13 A. Mondal, N. O. Thiel, R. Dorel and B. L. Feringa, *Nat. Catal.*, 2022, **5**, 10–19.

14 A. Mondal, V. Dašková, X. Chen, N. O. Thiel, G. Alachouzos and B. L. Feringa, *Chem. Commun.*, 2025, **61**, 6510–6513.

15 T. Lu and F. Chen, *J. Comput. Chem.*, 2012, **33**, 580–592.

16 (*a*) P. Liu, J. Montgomery and K. N. Houk, *J. Am. Chem. Soc.*, 2011, **133**, 6956–6959; (*b*) G. Lu, C. Fang, T. Xu, G. Dong and P. Liu, *J. Am. Chem. Soc.*, 2015, **137**, 8274–8283.

17 K. Li, N. Hu, R. Luo, W. Yuan and W. Tang, *J. Org. Chem.*, 2013, **78**, 6350–6355.

18 R.-R. Liu, Y.-G. Wang, Y.-L. Li, B.-B. Huang, R.-X. Liang and Y.-X. Jia, *Angew. Chem., Int. Ed.*, 2017, **56**, 7475–7478.

19 R.-X. Liang, K. Wang, Q. Wu, W.-J. Sheng and Y.-X. Jia, *Organometallics*, 2019, **38**, 3927–3930.

20 H.-R. Tong, S. Zheng, X. Li, Z. Deng, H. Wang, G. He, Q. Peng and G. Chen, *ACS Catal.*, 2018, **8**, 11502–11512.

21 (*a*) M. Gómez-Gallego and M. A. Sierra, *Chem. Rev.*, 2011, **111**, 4857–4963; (*b*) E. M. Simmons and J. F. Hartwig, *Angew. Chem., Int. Ed.*, 2012, **51**, 3066–3072.

22 (*a*) T. T. Tsou and J. K. Kochi, *J. Am. Chem. Soc.*, 1979, **101**, 6319–6332; (*b*) C. N. Pierson and J. F. Hartwig, *Nat. Chem.*, 2024, **16**, 930–937.

23 (*a*) L. Ackermann, *Acc. Chem. Res.*, 2020, **53**, 84–104; (*b*) N. Chatani, *Acc. Chem. Res.*, 2023, **56**, 3053–3064; (*c*) Y. H. Liu, Y.-N. Xia and B.-F. Shi, Ni-catalysed chelation-assisted direct functionalization of inert C−H bonds, *Chin. J. Chem.*, 2020, **38**, 635–662.

24 (*a*) D. Balcells, E. Clot and O. Eisenstein, *Chem. Rev.*, 2010, **110**, 749–823; (*b*) M. Garcia-Melchor, A. A. C. Braga, A. Lledós, G. Ujaque and F. Maseras, *Acc. Chem. Res.*, 2013, **46**, 2626–2634; (*c*) D. L. Davies, S. A. Macgregor and C. L. McMullin, *Chem. Rev.*, 2017, **117**, 8649–8709.

25 (*a*) CCDC 2442475: Experimental Crystal Structure Determination, 2026, DOI: 10.5517/ccdc.csd.cc2mzljr; (*b*) CCDC 2442477: Experimental Crystal Structure Determination, 2026, DOI: 10.5517/ccdc.csd.cc2mzllt; (*c*) CCDC 2442408: Experimental Crystal Structure Determination, 2026, DOI: 10.5517/ccdc.csd.cc2mzjcj; (*d*) CCDC 2442469: Experimental Crystal Structure Determination, 2026, DOI: 10.5517/ccdc.csd.cc2mzlbk.